Editors' Suggestion

Neutron-neutron scattering length from the ^{6}He$(p, p\alpha)nn$ reaction

Matthias Göbel [1,*] Thomas Aumann [1,2,3] Carlos A. Bertulani [4] Tobias Frederico [5]
Hans-Werner Hammer [1,6,3] and Daniel R. Phillips [7,1,6]

[1]*Technische Universität Darmstadt, Department of Physics, Institut für Kernphysik, 64289 Darmstadt, Germany*
[2]*GSI Helmholtzzentrum für Schwerionenforschung GmbH, Planckstraße 1, 64291 Darmstadt, Germany*
[3]*Helmholtz Research Academy for FAIR, 64291 Darmstadt, Germany*
[4]*Department of Physics and Astronomy, Texas A&M University-Commerce, Commerce, Texas 75429, USA*
[5]*Instituto Tecnológico de Aeronáutica, DCTA, 12.228-900 São José dos Campos, SP, Brazil*
[6]*ExtreMe Matter Institute EMMI, GSI Helmholtzzentrum für Schwerionenforschung GmbH, 64291 Darmstadt, Germany*
[7]*Institute of Nuclear and Particle Physics and Department of Physics and Astronomy, Ohio University, Athens, Ohio 45701, USA*

(Received 10 March 2021; revised 1 June 2021; accepted 6 July 2021; published 9 August 2021)

We propose a novel method to measure the neutron-neutron scattering length using the ^{6}He$(p, p\alpha)nn$ reaction in inverse kinematics at high energies. The method is based on the final-state interaction (FSI) between the neutrons after the sudden knockout of the α particle. We show that the details of the neutron-neutron relative-energy distribution allow for a precise extraction of the s-wave scattering length. We present the state of the art in regard to the theory of this distribution. The distribution is calculated in two steps. First, we calculate the ground-state wave function of ^{6}He as a αnn three-body system. For this purpose we use Halo effective field theory, which also provides uncertainty estimates for the results. We compare our results at this stage to model calculations done with the computer code FaCE. In a second step we determine the effects of the nn FSI using the nn t-matrix. We compare these FSI results to approximate FSI approaches based on standard FSI enhancement factors. While the final distribution is sensitive to the nn scattering length, it depends only weakly on the effective range. Throughout we emphasize the impact of theoretical uncertainties on the neutron-neutron relative-energy distribution, and discuss the extent to which those uncertainties limit the extraction of the neutron-neutron scattering length from the reaction ^{6}He$(p, p\alpha)nn$.

DOI: 10.1103/PhysRevC.104.024001

I. INTRODUCTION AND CONCLUSION

The significant difference between the proton-proton (pp) and the neutron-neutron (nn) interaction is a consequence of the charge symmetry breaking of the nucleon-nucleon (NN) interaction. It has its fundamental origin in the different masses and electromagnetic properties of the light quarks [1]. The charge symmetry breaking of the NN interaction is, for example, manifested in the s-wave scattering lengths that parametrize the zero-energy NN cross section. Because of their fundamental importance, the nn and pp scattering lengths have been a topic of intense research. The current accepted values are $a_{pp}^{\rm str} = (-17.3 \pm 0.4)$ fm and $a_{nn}^{\rm str} = (-18.9 \pm 0.4)$ fm [2–4]. The superscript "str" indicates that electromagnetic effects have been removed in these numbers, but in the remainder of the paper we actually use the raw quantities measured in experiment. The corresponding value for the nn interaction is $a_{nn} = (-18.6 \pm 0.4)$ fm.

It should be noted, however, that there is a systematic and significant difference between the extracted values of a_{nn} from neutron-induced deuteron breakup reactions measured by two different collaborations with different experimental setups. A group from Bonn has measured the $d(n, pn)n$ reaction and extracted $a_{nn} = -16.3(4)$ fm [5] using a theoretical analysis based on three-body Faddeev equations [6]. Different beam energies and analysis methods (absolute vs relative cross sections) yielded slightly different, but consistent, values for the scattering length. This result was confirmed (but with larger uncertainties) in a more recent measurement in Bonn using the same reaction but with only the final-state proton being detected [7]. Around the same time as the earlier Bonn experiment, a group from TUNL extracted the value $a_{nn} = -18.7(7)$ fm [8][1] from their experiment using the same reaction with all final particles detected and the same theoretical treatment. This value was later confirmed in a reanalysis of the TUNL experiment [9]. The discrepancy between the two values is an unsolved puzzle and points towards an unknown experimental systematic uncertainty.

An alternative method which avoids the complication of the hadronic three-body final state is given by the pion capture reaction $\pi^- d \to nn\gamma$. In this case, a slow pion is captured in a ^{2}H atomic state and then absorbed by the deuteron yielding the breakup into two neutrons and a photon. In some experiments only the high-energy photon is measured; in others the

*goebel@theorie.ikp.physik.tu-darmstadt.de

[1]The value is from Ref. [8], but the uncertainty band is from Ref. [9], where almost the same group published a reanalysis of the data.

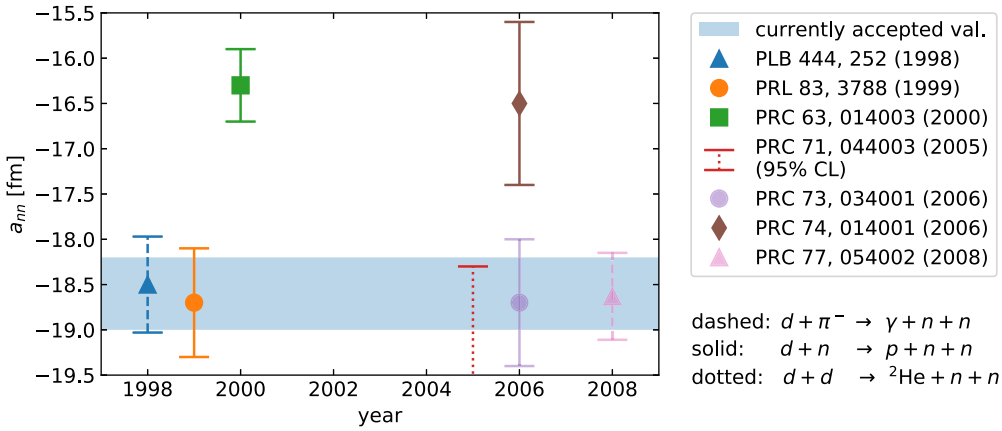

FIG. 1. Recent experimental data on the neutron-neutron scattering length, as reported in Refs. [5,7–9,14–17]. The horizontal band displays the uncertainty band of the accepted value, according to Refs. [2,3]. The line style of the error bar encodes information on the reaction; see legend. Results based on the same experimental data only differing in the analysis use the same point style. In the shown values for a_{nn}, effects of the magnetic-moment interaction are not removed; see, e.g., Ref. [2] for more details.

photon is measured in coincidence with one of the outgoing neutrons. The scattering length is extracted from a fit to the shape of the neutron spectrum, i.e., the decisive feature is the relative height of the quasifree $p\pi$ capture peak and the peak caused by final-state interaction (FSI). From the combination of experiments at PSI [10–13] and Los Alamos [14] $a_{nn} = -18.6(4)$ fm is deduced [3], which is in agreement with the deuteron breakup experiments at TUNL and presently considered the accepted value.

The most recent data for a_{nn} are displayed in Fig. 1 together with the limits of the accepted value (horizontal band). We also display there a result obtained at KVI from the reaction $^2\mathrm{H}(d,^2\mathrm{He})^2n$. Using a simple reaction model, they extracted an upper bound of -18.3 fm at the 95% confidence level.

The nn scattering length can be also inferred from pion photoproduction on deuterium $\gamma d \rightarrow \pi^+ nn$ as, e.g., Refs. [18–21] have shown. While the theoretical study in Ref. [20] used chiral perturbation theory for the regime of γ energies close to pion-photoproduction threshold, it is supplemented for higher γ energies by a recent study in Ref. [21] using a realistic model for this reaction. The determination of the nn scattering length with such an experiment can be realized by a precision measurement of the energies of the incoming γ and the outgoing π^+. The neutron detection efficiency is not problematic for this experimental method but an analysis of the theory uncertainties remains to be carried out.

In this paper we propose a novel method to measure a_{nn}. This method takes advantage of inverse kinematics at a ^{6}He beam energy of a few hundred MeV/nucleon. The ^{6}He beam impinges on a proton target, resulting in quasifree knockout of the α particle. The two halo neutrons of the ^{6}He projectile are liberated by this knockout, and both continue flying forward in the laboratory system with approximately beam velocity. Their relative energy remains small: it is determined by the overlap of the nn wave functions in the ^{6}He ground state and the nn scattering state, and so depends strongly on the nn scattering length at low relative energies. The neutrons are detected at approximately 10 m distance from the target around 0° with a 1×1 m^2 large detector array covering the nn relative-energy spectrum from 0 to 1 MeV. In addition to the two halo neutrons, both the α particle and proton are detected, allowing selection of events in which the charged particles are scattered to large angles. This quasielastic high-energy scattering process results in large relative energies between the charged particles and the neutrons: that this occurs is verified by the measurement of the tracks of the two scattered particles. Any non-nn final-state interactions are now again high-energy scattering processes, resulting in substantial changes of angles and relative energies between the particles. In particular, the neutrons will not remain in the low-relative-energy state ($E_{nn} < 1$ MeV) in the case of final-state interaction with the charged particles, and so will not be detected—and the kinematical signature of energies and angles of charged particles would also then not correspond to the quasielastic kinematics. Therefore, although the non-nn FSI is present, it results only in a reduction of observed events and does not distort the low-energy E_{nn} spectrum. Nowadays the relative energy between the high-energy neutrons can be measured with an energy resolution of about 20 keV, so the nn energy spectrum can be mapped out with high accuracy. In this paper we argue that the imprint of a_{nn} on that low-energy nn (relative) energy spectrum far exceeds uncertainties coming from the ^{6}He structure and the reaction dynamics. And, because all four final-state particles are detected, a background-free measurement can be performed. We conclude that this kind of $^6\mathrm{He}(p, p\alpha)nn$ measurement can be used to extract the neutron-neutron scattering length. A proposal to carry out such an experiment has been approved at RIKEN [22].

In contrast to the novel method proposed in this paper, previous extractions of a_{nn} relied on measuring the intensity of the neutron-neutron FSI peak relative to the quasifree peak. These are located at rather different neutron energies. In our proposal, the neutrons originating from the projectile have a high and almost constant velocity avoiding possible sources of systematic uncertainties due to energy-dependent corrections for neutron efficiency, scattering, and attenuation in the target, etc., as were necessary in the previous experiments.

It is clear that a general description of the ^{6}He$(p, p\alpha)nn$ knockout reaction is a formidable task. However, we stress that the proposal is to extract a_{nn} in high-energy kinematics where we argue that the a_{nn} dependence of the relative-energy distribution of the neutrons can be calculated reliably and with quantified theoretical uncertainties. An analogous extraction could be made in the $t(p, 2p)nn$ knockout reaction as a cross-check, but we will not consider that reaction in this paper.

The calculations presented below demonstrate the sensitivity of the nn relative-energy distribution in ^{6}He$(p, p\alpha)nn$ to the nn scattering length. In Sec. V we show that varying the nominal scattering length of -18.7 fm by 2 fm changes characteristic parts of the distribution around $E_{nn} = 100$ keV by roughly 10%. This sensitivity will enable a precise experimental determination of the scattering length. Furthermore, the spectrum has only a small dependence on the nn effective range: we find that its effect is less than 1%. We now lay out the procedure and assumptions through which we calculate the nn relative-energy distribution. We also summarize here the uncertainties associated with each piece of our calculation.

(1) In Secs. II and III we describe and present results from our computation of the ground-state momentum distribution of ^{6}He, i.e., the distribution in the absence of final-state interactions. We treat the nucleus as a αnn three-body system and use both an effective field theory (EFT) of the halo nucleus [23,24] and a three-body model. The EFT calculation is carried out at leading order (LO) and has a nominal uncertainty of $\approx 20\%$ for $E_{nn} \approx 1$ MeV. We compare the EFT momentum distribution to that obtained with a three-body model of ^{6}He that uses local Gaussian two-body potentials as well as a three-body force. This "LGM" calculation is in the tradition of, e.g., Refs. [25,26], and is implemented via the computer code FaCE [27]. The resulting momentum distribution is consistent with that obtained from the Halo EFT within the expected uncertainty of a leading-order calculation. At next-to-leading order the EFT uncertainty band will be smaller and better agreement is expected. We analyze which effects cause the differences between the EFT and LGM distribution and show that corrections to the nc t-matrix are the most significant next-to-leading-order (NLO) corrections to the structure of ^{6}He in the EFT approach.

(2) In treating the reaction dynamics we assume the knockout of the α by the proton results in its sudden removal and does not distort the E_{nn} spectrum. To some degree this can be ensured during the analysis of the experimental data by taking only those events where the measured charged particles meet the necessary kinematical conditions. Nevertheless, assessing the error induced in the neutron-neutron relative-energy spectrum by this use of the sudden approximation is an important topic for future work.

(3) At the moment only nn FSI is taken into account. The reason that the distortion effect due to αn or pn FSI is higher order is the smallness of the effect in the chosen kinematics according to scaling arguments. The αn FSI is suppressed by the ratio p_{nn}/k, where p_{nn} and k are the relative momentum between the two neutrons and the momentum transfer to the α particle, respectively. The experiment in the proposed kinematics selects by construction small p_{nn} and large k, resulting in the suppression of effects due to FSI between the neutrons with the charged particles involved in the reaction. Any remaining correction, if necessary, will be small, so that the accuracy of calculating the correction does not have to be high to fulfill the precision requirement of the analysis of experiment and the extraction of a_{nn}.

(4) Under the assumptions of the previous two points the nn relative-energy distribution is straightforwardly obtained from the ^{6}He wave function using a two-body treatment of FSI. In Sec. IV we compare results based on a full calculation of the nn FSI using the t-matrix to approximate results based on so-called enhancement factors. We discuss the derivation of the latter technique, which was established by Watson [28] and Migdal [29]. (Reviews can be found in Refs. [30,31].) By formulating the problem in terms of two-potential scattering theory we show that the enhancement factors are approximations to an exact calculation of nn FSI via the t-matrix. This establishes a preference for the t-matrix approach. But, regardless of that preference, the calculations of Sec. IV show that the key parts of the distribution around $E_{nn} = 100$ keV that change by roughly 10% if a_{nn} is varied by 2 fm (see Sec. V) are moderately insensitive to the approach used for the nn final-state interaction. We conclude that the impact of different treatments of nn FSI on the error budget of the a_{nn} extraction is minimal.

(5) Our calculations of the neutron energy distribution after α-particle knockout use only the partial-wave state where the nn system and the $(nn) - c$ system are both in a relative s wave. This is the most important component in our calculation of the ground state, and the nn FSI increases its dominance. We quantitatively assessed the relevance of the other components and found that in the case of a LGM calculation with nn FSI the contribution to the nn energy distribution for $E_{nn} < 1$ MeV from two neutrons in a relative $^3P_1$ wave is at least a factor of 30 smaller than that that from the $^1S_0$ wave.

Having laid out the procedure for calculating the nn relative-energy distribution in Secs. II–IV, in Sec. V we investigate the sensitivity of that distribution to the scattering length. We close in Sec. VI with an outlook regarding future calculations.

II. THREE-BODY CALCULATIONS OF ^{6}He

The first step for obtaining the nn relative-energy distribution is obtaining the ground-state wave function of ^{6}He. Because of its halo structure it can be described as a αnn three-body system. The halo structure manifests itself in a two-neutron separation energy, which corresponds to the binding energy of the αnn three-body system, $B_3^{(0)} = 0.975$ MeV [32], much smaller than the α core's excitation energy $E_\alpha^* \approx 20$ MeV. We calculate the wave function in Halo EFT at leading order and compare to results obtained in three-body model calculations of the system. In this section, we introduce concepts and quantities necessary for both methods. The relative positions and momenta can be described by splitting the three-body system into a two-body system and a third particle. The momenta are then given in terms of the relative momentum between the constituents of the subsystem and the relative momentum between the third particle and the center of mass of the subsystem. In position space, the coordinates can be

chosen analogously. The third particle is called the spectator, and its choice is arbitrary. These momenta are called Jacobi momenta. The Jacobi momenta of the three-body system with momenta k_i and masses m_i ($i \in \{1, 2, 3\}$) are given by

$$\boldsymbol{p}_i \coloneqq \mu_{jk}\left(\frac{\boldsymbol{k_j}}{m_j} - \frac{\boldsymbol{k_k}}{m_k}\right), \quad \boldsymbol{q}_i \coloneqq \mu_{i(jk)}\left(\frac{\boldsymbol{k_i}}{m_i} - \frac{\boldsymbol{k_j}+\boldsymbol{k_k}}{M_{jk}}\right), \quad (1)$$

where the definitions $\mu_{ij} \coloneqq (m_i m_j)/(m_i + m_j)$, $\mu_{i(jk)} \coloneqq (m_i M_{jk})/(m_i + M_{jk})$, and $M_{ij} \coloneqq m_i + m_j$ hold.[2] In order to describe this three-body system in a partial-wave basis we have to assign quantum numbers. With the coordinates, they generally depend on the chosen spectator. The relative orbital angular momentum quantum number of the subsystem is given by l; the one between the third particle and the subsystem is given by λ. The quantum number s specifies the total spin of the subsystem, while σ denotes the spin of the third particle. In $\boldsymbol{jJ}$ coupling the relations $\boldsymbol{j} = \boldsymbol{l} + \boldsymbol{s}$ and $\boldsymbol{I} = \boldsymbol{\lambda} + \boldsymbol{\sigma}$ hold. A general partial-wave state reads

$$|(l, s)j, (\lambda, \sigma)I; J, M\rangle_i, \quad (2)$$

where the index i on the right specifies the spectator.

Before going into the specifics of the three-body calculations, we want to discuss the reference states for calculating the ground-state wave function. Since we are investigating ground states, we have in the case of ^{6}He the condition $J = M = 0$. The spin of the α particle is zero. This implies $\sigma = 0$ in the case of the α particle as spectator (indicated by an index c for core at the bra/ket). The two neutrons with spin 1/2 can couple to 0 or 1, meaning that s is 0 or 1. Under these conditions four different types of partial-wave basis states can be formed; states of each type are parametrized by the orbital angular momentum quantum number of the subsystem l. If $s = 0$, the states are of the form

$$\left|\Omega_c^{(0,l,l)}\right\rangle_c \coloneqq |(l, 0)l, (l, 0)l; 0, 0\rangle_c \quad \text{with } l \geqslant 0. \quad (3)$$

For $s = 1$ the following three types of states can be formed:

$$\left|\Omega_c^{(1,l,l-1)}\right\rangle_c \coloneqq |(l, 1)l-1, (l-1, 0)l-1; 0, 0\rangle_c, \quad l \geqslant 1, \quad (4)$$

$$\left|\Omega_c^{(1,l,l)}\right\rangle_c \coloneqq |(l, 1)l, (l, 0)l; 0, 0\rangle_c, \quad l \geqslant 1, \quad (5)$$

$$\left|\Omega_c^{(1,l,l+1)}\right\rangle_c \coloneqq |(l, 1)l+1, (l+1, 0)l+1; 0, 0\rangle_c, \quad l \geqslant 0. \quad (6)$$

This produces a complete, orthogonal angular momentum basis for a three-body system of $J = M = 0$ that is formed out of two distinguishable spin-$\frac{1}{2}$ particles and one spin-zero particle. In the following we will call these basis states "reference states" and calculate their overlaps with the eigenstate of the three-body Hamiltonian in order to obtain wave functions on the partial-wave basis.

The ground state of ^{6}He has positive parity and is antisymmetric under interchange of the two neutrons. Only the piece of a reference state with the same symmetries as the ground state will have nonvanishing overlap with it. Therefore, $\Omega_c^{(1,l,l-1)}$ and $\Omega_c^{(1,l,l+1)}$ are not suitable reference states, as they have negative parity. Similarly, the requirement of nn antisymmetry means that we only need to consider states $\Omega_c^{(0,l,l)}$ where the quantum number l is even, together with states $\Omega_c^{(1,l,l)}$ where l is odd. This analysis of the possible states is consistent with other three-body calculations of the ground state of ^{6}He presented, e.g., in Refs. [25,26].

A. Local Gaussian model

Our model calculation of the three-body system employs commonly used local l-dependent Gaussian potentials as well as a three-body force. We call this a local Gaussian model (LGM). To solve it for the three-body system we use the computer code FaCE [27].[3] It calculates the position-space wave function of a three-body system by solving the Schrödinger equation with local l-dependent two-body interactions and phenomenological three-body potentials. It is capable of removing unphysical bound states from two-body potentials via the supersymmetric (SUSY) transformations described in Ref. [36]. The name FaCE is an acronym for "Faddeev with core excitation." It alludes to the fact that in the default setting it solves not the Schrödinger equation but the equivalent Faddeev equations.[4] As the name also expresses core excitation effects can be taken into account within this code.

This code and its ancestors were used for calculations of multiple nuclei. In the case of ^{6}He, the position-space probability densities and transverse-momentum distributions were already calculated with ancestors of the FaCE code, e.g., in Refs. [25,26]. The results for the transverse momentum distribution agree well with available experimental data.

We now define the parameters that are specified in a typical FaCE input file for ^{6}He, and in the process also write down the potentials employed in our LGM for this system. For the nn interaction as well as the $n\alpha$ interaction we use local central and spin-orbit potentials:

$$\langle r; l, s|V_c^{(\tilde{l})}|r'; l', s'\rangle \coloneqq \delta_{l,l'}\delta_{l,\tilde{l}}\delta_{s,s'}\frac{\delta(r'-r)}{r'^2}\bar{V}_c^{(l)}\exp\left[-r^2/\left(a_{c;l}^2\right)\right], \quad (7)$$

$$\langle r; l, s|V_{\mathrm{SO}}^{(\tilde{l})}|r'; l', s'\rangle \coloneqq \delta_{l,\tilde{l}}\frac{\delta(r'-r)}{r'^2}\bar{V}_{\mathrm{SO}}^{(l)}\langle l, s|\boldsymbol{LS}|l', s'\rangle\exp\left[-r^2/\left(a_{\mathrm{SO};l}^2\right)\right], \quad (8)$$

where the depth parameters are denoted by $\bar{V}_c^{(l)}$ and $\bar{V}_{\mathrm{SO}}^{(l)}$. The range parameters are given by $a_{c;l}$ and $a_{\mathrm{SO};l}$.

[2]Note, that, e.g., in Ref. [26] a different convention for the Jacobi momenta is used. Some notes on the differences can be found in the Supplemental Material [33]. We use the convention which is used, e.g., in Refs. [23,24,34].

[3]The code itself can be obtained from a research data repository [35].

[4]Note that the Faddeev equations which are used by FaCE are equivalent to the ones used in our EFT calculation. However they are not of the same form. FaCE uses matrix elements of potentials; the EFT calculation uses matrix elements of t-matrices. These two versions of the Faddeev equations have the decomposition of the total state into components in common.

In the LGM calculation the *nc* interaction is present in the *s* wave, *p* wave, and *d* wave. In the *p* wave and *d* wave both central potentials and spin-orbit potentials are used. A *p*-wave nucleon-α potential of this form was first specified in Ref. [37], where it was shown to provide a reasonable description of low-energy $p\alpha$ phase shifts. Here we take for all *nc* potentials a range of $a_{c;l} = a_{\mathrm{SO};l} = 2.3$ fm. The depth parameters are $\bar{V}_{c;0} = \bar{V}_{c;1} = -47.32$ MeV, $\bar{V}_{\mathrm{SO};1} = \bar{V}_{\mathrm{SO};2} = -11.71$ MeV, and $\bar{V}_{c;2} = -23.0$ MeV. These parameters except the *s*-wave ones were *inter alia* used for the calculation with an ancestor of FaCE in Ref. [26] and presumably in Ref. [25] as well as in the recent Ref. [38]. In the case of the *s* wave we do not use the repulsive potential used in Ref. [26]. Instead, we follow the FaCE sample input file for ^{6}He which means we use the previously mentioned attractive potential and remove the unphysical $n\alpha$ bound state using the SUSY transform capabilities of FaCE. This attractive potential produces a satisfactory fit to the phase shifts given in Ref. [39].

For the *nn* interaction we use a *s*-wave central potential with the parameters $\bar{V}_{c;0} = -31.0$ MeV and $a_{c;0} = 1.8$ fm. These parameters were also used *inter alia* for the calculation in Refs. [26,38] and are taken from Ref. [40].

The phenomenological three-body force reads

$$V_{3\mathrm{B}}(\rho) := \frac{s_{3\mathrm{B}}}{1.0 + (\rho/\rho_{3\mathrm{B}})^{a_{3\mathrm{B}}}}. \tag{9}$$

The parameters $\rho_{3\mathrm{B}} = 5.0$ fm and $a_{3\mathrm{B}} = 3$ are used, as they are set in the sample input file of FaCE. The depth parameter $s_{3\mathrm{B}}$ will be tuned to reproduce $B_3^{(0)}$.

FaCE calculates the wave functions of three-body systems such as ^{6}He in terms of a decomposition in the hyperangular momentum K. The single components are specified by the hyperangular momentum quantum number and the angular and spin quantum numbers. By doing the decomposition in K, the wave function's coordinate-space dependence on x and y, which are conjugate to p and q, can be replaced by the dependence on the hyper-radius $\rho := \sqrt{x^2 + y^2}$. In the following these wave-function components $\chi_K(\rho)$ will have only the additional indices l and S, as, due to the symmetries discussed in the beginning of this section, these determine all other quantum numbers of the ^{6}He ground state with $J = M = 0$ and positive parity in $\boldsymbol{jJ}$ coupling: $\lambda = l$, $s = S$, $\sigma = 0$, and $j = I = l$ (core as spectator). The *nn* relative-momentum distribution is calculated using the momentum-space wave function, while the calculation of this wave function from $\chi^S_{K,l}(\rho)$ is summarized in the Supplemental Material [33]. It contains also details on the computational parameters of the model calculation.

B. Halo EFT approach

A second approach for obtaining the three-body wave function of ^{6}He is using Halo effective field theory (Halo EFT). An effective field theory is a toolkit for exploiting the scale separation of a physical system in order to calculate observables as a series in the ratio of a typical momentum scale over a high-momentum scale. The high-momentum scale is the lowest scale of omitted physics. Systematic improvement of the results is then possible by calculating higher orders in the expansion. And at any given order the EFT's expansion in a ratio of momentum scales enables robust uncertainty estimates for its predictions.

Halo EFT is a pionless EFT describing halo nuclei. The halo nucleons are associated with the lower momentum scale while the high momentum is associated with effects such as pion creation, removal of nucleons from the core, or excitation of the core. In the case of ^{6}He the low-momentum scale M_{low} can be determined, using the three-body binding energy $B_3^{(0)} = 0.975$ MeV, to be $M_{\mathrm{low}} = \sqrt{m_n B_3^{(0)}} \approx 30$ MeV. The high-momentum scale is given by $M_{\mathrm{high}} = \sqrt{m_n E_\alpha^*} \approx 140$ MeV, where the excitation energy of the core is given by $E_\alpha^* \approx 20$ MeV. The basic ingredient of an EFT calculation is the power counting. It tells which terms are of which order in $M_{\mathrm{low}}/M_{\mathrm{high}}$ and thereby defines which have to be included in a calculation at a given order. The $n\alpha$ system was first investigated in a Halo EFT framework in Refs. [41,42], which proposed different power countings: Ref. [41] proposes $a_1 \sim M_{\mathrm{low}}^{-3}$ and $r_1 \sim M_{\mathrm{low}}$, where a_1 is the *p*-wave scattering volume and r_1 is the *p*-wave effective range. Usually one expects that the effective range parameters are of order of the appropriate power of M_{high}, thereby we have two fine-tunings here. According to the power counting of Ref. [42] $a_1 \sim M_{\mathrm{low}}^{-2} M_{\mathrm{high}}^{-1}$ and $r_1 \sim M_{\mathrm{high}}$ hold. This power counting has the minimum number of fine-tunings necessary to produce a bound state or resonance in the low-energy region of the EFT.

The latter power counting was used in Ref. [23], where Halo EFT was applied to ^{6}He. In that paper the two-body subsystems as well as the three-body system were successfully renormalized. In order to renormalize the three-body system with a three-body force the binding energy $B_3^{(0)}$ was used as input. Additionally, Faddeev amplitudes were calculated and their independence of sufficiently high cutoffs was demonstrated. This paper was continued in Ref. [24], where ground-state probability densities were calculated in Halo EFT. The potentials corresponding to the leading-order t-matrices used in Refs. [23,24] are energy dependent. While in the case of the *s*-wave *nn* interaction this dependence vanishes in the limit that the cutoff goes to infinity, in the case of the *p*-wave *nc* interaction it does not vanish. In Refs. [43,44] quantum mechanics with energy-dependent potentials is discussed. *Inter alia* a modified normalization condition for wave functions is derived. These findings were applied to the calculation of the probability density in Ref. [24], where it was found that these modifications are negligible in the low-energy region. Furthermore, the robustness of the results with respect to the regulator was checked. The probability density is independent of the cutoff and the form of the momentum-space regulator.

In this paper, we use Halo EFT to calculate the ground-state wave function of ^{6}He. We base our calculation on the methodology used in Ref. [24]. We will solve the same Faddeev equations as in Ref. [24]; the only difference is that we will not calculate overlaps of plane wave states with $|\Psi\rangle$ but overlaps of partial-wave states with $|\Psi\rangle$. Since partial-wave states were also widely used in that paper, many formulas can be reused. At this point, we briefly review the Faddeev equations. While they can be derived in a nonrelativistic (effective) field

theory (see, e.g., Ref. [34]), we describe here the connection to the Schrödinger equation. This allows for straightforward comparisons with quantum mechanical model calculations. The Schrödinger equation for a three-body system with a kinetic Hamilton operator H_0, two-body interactions V_i, and a three-body potential V_3 reads

$$\left(H_0 + \sum_i V_i + V_3\right)|\Psi\rangle = E_3|\Psi\rangle, \tag{10}$$

where E_3 is the energy of the three-body system. The index i is the index of a third particle defining the subsystem consisting of the remaining particles, in which V_i acts. Accordingly $i \in \{c, n, n'\}$ holds. For the moment we consider the system without the three-body force. The Schrödinger equation can be rewritten into a set of coupled equations, the so-called Faddeev equations, for the Faddeev amplitudes $|F_i\rangle$ (see, e.g., Refs. [23,45,46]):

$$|F_i\rangle = \sum_{j\neq i} G_0 t_j |F_j\rangle, \tag{11}$$

where the connection to the desired $|\Psi\rangle$ is given by

$$G_0 t_i |F_i\rangle = G_0 V_i |\Psi\rangle, \tag{12}$$

$$\sum_i G_0 t_i |F_i\rangle = |\Psi\rangle. \tag{13}$$

We will use the latter equation in order to obtain the ground-state wave function from the Faddeev amplitudes. When we solve the Faddeev equations numerically, we have to use a representation of the states. It is common to use the following representation for $|F_i\rangle$:

$$F_i(q) = \int dp p^2 g_{l_i}(p) {}_i\langle p, q; \Omega_i | F_i\rangle, \tag{14}$$

where we assumed that V_i acts only in one partial-wave channel given by the set of quantum numbers Ω_i seen from particle i and that it has a one-term separable form in the corresponding two-body subsystem.

The three-body force can be included in the Faddeev formalism in several ways. One way is to modify Eq. (11) and leave the relation of obtaining the full states from the Faddeev amplitudes, namely, Eq. (13), unchanged [46]. We use this method, the employed three-body force is given in Ref. [23]. Alternative possibilities for this force in the case of ^{6}He can be found in Ref. [47].

We now give some more details on the used two-body interactions. Since we solve Faddeev equations in momentum space, which are equivalent to the Schrödinger equation, the two-body interactions are specified in the form of t-matrices. The real part of the denominator of the t-matrix corresponds to an effective-range expansion, which is carried out up to a certain order that is determined by the power counting of the EFT and the order of the calculation. But this does not determine the (off-shell) t-matrix. For convenience in the implementation of the Faddeev equations, we use separable t-matrices corresponding to separable potentials. This is a common choice; see, e.g., Refs. [23,24]. The elements of the t-matrix describing the interaction between particles i and j read

$$\langle p, l | t_{ij}(E) | p', l'\rangle = 4\pi \delta_{l,l'} \delta_{l_{ij},l} g_{l_{ij}}(p) \tau_{ij}(E) g_{l_{ij}}(p'), \tag{15}$$

where l_{ij} specifies the quantum number l of the interaction channel. The functions $g_l(p)$ are regulator functions specifying the damping at and above momenta of the order of the cutoff scale β parametrizing these functions. Additionally, they determine the off-shell behavior of the t-matrices. We use $g_l(p) = p^l \theta(\beta - p)$. For our three-body calculation we have to embed the t-matrix into the three-body system and take matrix elements of this embedded version. We obtain for the elements of the matrix t_i describing the interaction given by spectator i, i.e., the one between j and k, the following expression:

$$\begin{aligned} &{}_i\langle p, q; \Omega | t_i(E_3) | p', q'; \Omega'\rangle_i \\ &\quad = \delta_{\Omega,\Omega'} \delta_{\Omega,\Omega_i} \langle p, l_i | t_{jk}\left(E_3 - \frac{q^2}{2\mu_{i(jk)}}\right) | p', l_i\rangle, \end{aligned} \tag{16}$$

where $l_i = l(\Omega_i)$ is the subsystem orbital angular momentum quantum number of the interaction channel given by the multi-index Ω_i. The reduced t-matrix elements $\tau_{jk}(E)$ contain the first terms of the effective range expansion in their denominators. In our leading-order Halo EFT for ^{6}He, they are given by

$$\tau_{nn}(E) = \frac{1}{4\pi^2 \mu_{nn}} \frac{1}{\gamma_0 + ik}, \tag{17}$$

$$\tau_{nc}(E) = \frac{1}{4\pi^2 \mu_{nc}} \frac{1}{\gamma_1 \left(k^2 - k_R^2\right)}, \tag{18}$$

whereby the relation $k = \sqrt{2\mu_{jk} E}$ holds. The parameter γ_0 is the momentum of the *nn* virtual state and at leading order is given by the *nn* scattering length via $\gamma_0 = a_0^{-1}$. In contrast to the *nn* interaction, the p-wave τ_{nc} does not contain a unitarity term at leading order according to the power counting. The *nc* interaction is parametrized by the effective range expansion parameters a_1 and r_1 via $\gamma_1 = -r_1/2$ and $k_R = \sqrt{2/(a_1 r_1)}$, whereby k_R is the momentum of the low-energy resonance. The values $r_1 = -174.0227$ MeV and $k_R = 37.4533$ MeV were used. They can be obtained from the a_1 and r_1 given in Ref. [48]. The core mass is approximated by $m_c \approx 4m_n$.

After discussing the interactions, we briefly describe how the wave functions are obtained. From the system of equations for the Faddeev amplitudes given in Eq. (11) one obtains a coupled system of integral equations by using the representations given in Eq. (14). By discretizing the function it turns into an eigenvalue problem which is solved numerically. Based on the results for the Faddeev amplitudes the wave function can be calculated; details can be found in Appendix A. We check the convergence of the results for the wave functions and other quantities by varying the number of mesh points used for this discretization and for subsequent integrations.

In addition to the scale β that parametrizes the scale at which the regulator function $g_l(p)$ cuts off the two-body t-matrix in Eq. (15) we also place a cutoff Λ on the momentum-space integral equations obtained from Eq. (11) by using Eq. (14). We vary these two-body and three-body

cutoffs and assess how sensitive our predictions are to that variation. Typically we use the same value for both cutoffs.

III. GROUND-STATE *nn* RELATIVE-MOMENTUM DISTRIBUTION

We compare ground-state *nn* relative-momentum distributions obtained with Halo EFT and with LGM . By doing so, we can analyze and understand the uncertainty in the ground-state momentum distribution, which is an important ingredient for the final distribution after the knockout. As a preparation, we discuss the details of our definition of the distribution.

In the beginning of Sec. II, the reference states for obtaining wave functions in a partial-wave basis were discussed. Symmetry considerations yielded that only $\Omega_c^{(0,l,l)}$ (l is even) and $\Omega_c^{(1,l,l)}$ (l is odd) are relevant. Using these different reference states yields complementary information due to the orthogonality of their angular and spin part. We calculated wave functions in our leading-order Halo EFT framework using both sets of states for low l in the low-energy region up to roughly 140 MeV. As expected, the importance of wave-function components decreases with increasing l. And in fact, only the wave-function component with partial-wave quantum numbers $\Omega_c^{(0,0,0)}$ is relevant in this region. All other components are suppressed in this region by a factor of approximately 20, or even more.

Therefore in what follows we define the wave function

$$\Psi_c(p,q) \coloneqq {}_c\langle p,q;\Omega_c^{(0,0,0)}|\Psi\rangle. \tag{19}$$

For simplicity we sometimes use the abbreviated symbol $\Omega_c \coloneqq \Omega_c^{(0,0,0)}$ in what follows. The corresponding ground-state *nn* relative-momentum distribution is given by

$$\rho(p_{nn}) \coloneqq \int dq q^2 p_{nn}^2 |\Psi_c(p_{nn},q)|^2. \tag{20}$$

In the case of LGM, the suppression of the other wave functions compared to the wave function with the quantum numbers $\Omega_c^{(0,0,0)}$ is generally not as strong as in the case of the LO Halo EFT calculation. Nevertheless, in order to do an appropriate comparison, also for the LGM we calculate only this wave-function component. This choice is also motivated by the fact that after the *nn* final-state interactions the dominance of the component $\Omega_c^{(0,0,0)}$, where the *nn* pair is in ${}^1S_0$, is even increased in the low-energy region, as the *nn* interaction is much stronger in this partial wave.

Note that we have developed a cross-check for our results for ground-state *nn* relative-momentum distributions $\rho(p_{nn})$ obtained in LGM. We calculate $\langle r_{nn}^2\rangle$ for different partial waves l using the relation

$$\langle r_{nn}^2\rangle_l = -\frac{\pi}{4}\left(\int dp_{nn}\partial_{p_{nn}}^2\rho_l(p_{nn}) - 2(1+l(l+1)) \times \int dp_{nn}\frac{\rho_l(p_{nn})}{p_{nn}^2}\right) \tag{21}$$

and compare the overall result with the results from Ref. [26], where $\langle r_{nn}^2\rangle$ and other observables were obtained in similar model calculations.

A. Comparison of results

Figure 2 shows the LGM result for the ground-state *nn* relative-momentum distribution in comparison with the leading-order Halo EFT result. They are normalized to have a certain arbitrary value at a certain position. We use this normalization procedure, as the absolute value is not necessary for determining the scattering length. More information on that can be found in Sec. V. This also avoids the difficulty that the norm of the EFT results depends on values of the wave function outside its range of validity. The uncertainty band of the EFT result is based on the size of the next-to-leading-order corrections. They are suppressed by p/M_{high}. Accordingly the uncertainty is $\Delta\rho(p) \approx \rho(p)\frac{p}{M_{\text{high}}}$. In the left panel (a) it can be seen that EFT and LGM results agree within the uncertainty bands of the LO Halo EFT result. The EFT distribution has generally bigger values and its maximum is at higher momenta. In higher-order Halo EFT calculations, the uncertainty bands (i.e., the relative uncertainty) will get smaller. Agreement between that higher-order Halo EFT calculation and LGM result is expected within this smaller uncertainty band. That implies that NLO corrections will move the Halo EFT result towards the LGM one, although at some high order no further improvement of agreement can be expected. Eventually, the assumptions of the model calculation will become visible in terms of small insurmountable differences between a high-order EFT and a model calculation. The right panel (b) shows that the agreement is, as expected, better in the low-energy region. Importantly, the determination of the *nn* scattering length involves measuring the distribution only up to $E_{nn} \approx 1$ MeV, i.e., the region where the agreement is especially good.

This comparison shows the consistency of the results. But we are interested in the sources of the discrepancies and in what results we can expect from a Halo EFT calculation at next-to-leading order. There are several possible sources for the discrepancies, such as the phenomenological LGM three-body potential, different effective-range-expansion parameters, or different off-shell properties of the two-body interactions that are not compensated by the used three-body forces (see Ref. [49] for details on this topic). Additionally, the discrepancies can be caused by terms which are part of higher-order EFT descriptions, e.g., the unitarity term of the *nc* system or interactions in additional partial waves such as ${}^2P_{1/2}$ and ${}^2S_{1/2}$ in the *nc* system. In order to estimate the importance of these different effects, we performed additional model calculations. We introduced modified versions of LGM that have fewer *nc* interaction channels (LGM2) or in which the three-body potential is completely absent or of shorter range. The LGM2 calculations show that the LGM result gets more similar to the EFT one if the *nc* interactions are turned off in channels other than the ${}^2P_{3/2}$ (see Fig. 3). The *s*-wave, *d*-wave, and ${}^2P_{1/2}$ *nc* interactions, which in the EFT are higher-order effects, are therefore causing part of the discrepancy. Meanwhile, calculations using other LGM variants (see Supplemental Material [33]) show that the phenomenological LGM three-body force is an important ingredient: if it is omitted, the gap with the EFT result increases. However, the range of the LGM three-body force seems to play only a

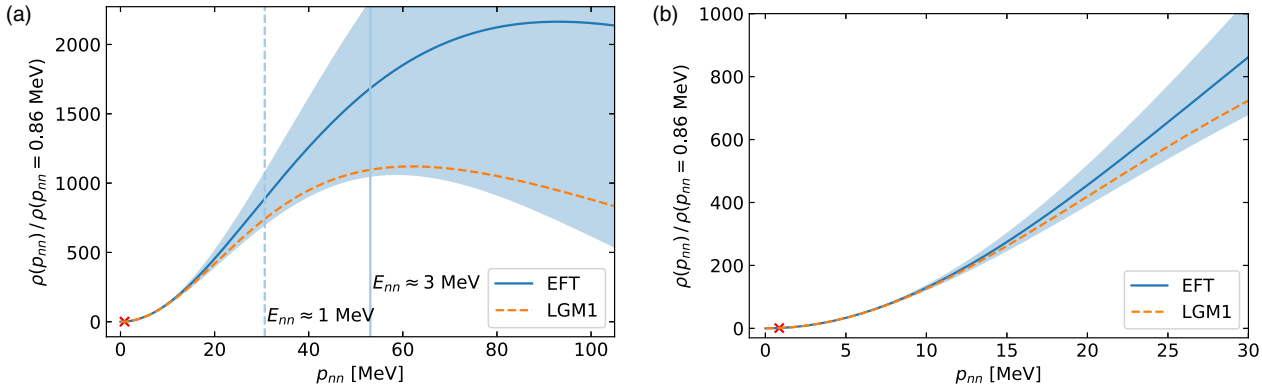

FIG. 2. LGM result in comparison with the Halo EFT result. The three-body potential in the LGM calculation was tuned to reproduce $B_3^{(0)}$. The used settings for LGM are denoted by LGM1. In order to be independent of the normalization the distributions are divided by their value at a certain position, which is indicated by the red cross. Note the dashed and solid vertical lines in the left panel (a). They indicate relative energies of 1 and 3 MeV, respectively. In the planned experiment 1 MeV will be roughly the upper bound of the measurement range.

small role. Using a value of 2.5 fm instead of 5 fm for ρ_{3B} has only a small effect on the LGM result, provided the three-body force's strength is adjusted to reproduce the physical binding energy of the three-body system.

While the interactions for the LGM calculations are specified in terms of coordinate-space matrix elements of potentials, momentum-space t-matrices are used for the EFT calculations. In order to connect the EFT calculations to a model, we also performed calculations using a model formulated directly in momentum space. This can be achieved by using our computer code for the EFT calculations with different separable t-matrices. The resulting model calculation has the same interaction channels as Halo EFT at LO and is similar to those of Refs. [50–52]. We chose separable t-matrices with Yamaguchi form factors, with interaction parameters adjusted to reproduce effective-range-expansion parameters. This yields reasonable phase shifts. In a first step, we compared the Yamaguchi model (YM) results with our EFT and LGM results. We found that the YM results for the ground-state momentum distribution are much more similar to the results from LGM2 (LGM with the reduced set of interaction channels) than to the EFT results. This implies that if we understand the discrepancy between YM and EFT we also understand the discrepancy between LGM and EFT.

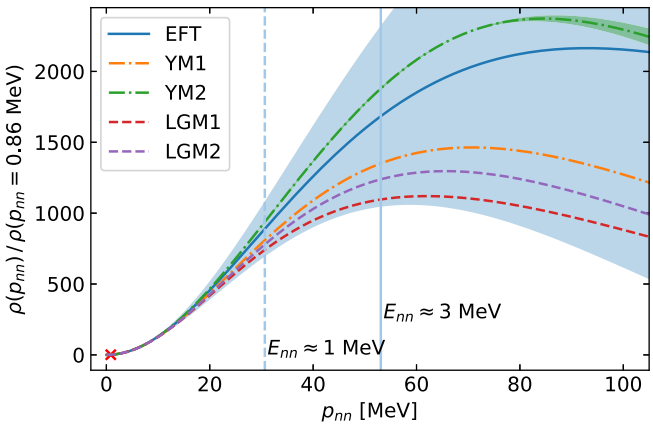

FIG. 3. YM results (dot-dashed lines) in comparison with the LO Halo EFT result (solid line) as well as LGM results (dashed lines). All are normalized to have a certain arbitrary value at a momentum indicated by the red cross. Meanwhile, the vertical dashed and solid lines indicate, respectively, relative energies of 1 and 3 MeV. The estimated numerical uncertainty of the YM2 result is indicated by the green band, while the one of the YM1 result is smaller than the line width. The uncertainty bands are estimated by varying the three-body cutoff from 1500 MeV to 2250 MeV and by varying the number mesh points by a factor of 2. The light blue error band for the Halo EFT result shows the expected size of the NLO correction.

Figure 3 shows the standard LGM and YM calculations, labeled LGM1 and YM1. The LGM calculation with a reduced set of channels (LGM2) is also shown. In addition, we perform a YM calculation with the unitarity term of the *nc* t-matrix removed, while other higher-order terms which are part of the YM but are not in the LO Halo EFT calculation are retained (YM2). The YM2 calculation comes out quite close to the LO Halo EFT result, indicating that the unitarity term in the *nc* t-matrix, which is an NLO effect in the EFT, has a significant influence on the ground-state momentum distribution and causes a large fraction of the YM-EFT difference. This implies that the NLO Halo EFT calculation will likely agree much better with a YM or LGM calculation than the LO Halo EFT does.

To conclude this subsection, the comparison between EFT and LGM1 yields agreement at the expected level: the EFT uncertainty bands are indeed robust. We expect the NLO Halo EFT result to be closer to this model that includes additional effects, and we tracked down the specific NLO term that should most improve agreement. Comparisons with additional model calculations indicate that the unitarity term of the *nc* interaction plays a significant role in this distribution. A more detailed analysis of the differences and additional plots can be found in the Supplemental Material [33].

B. Influence of the *nn* scattering length on the ground-state momentum distribution

Up to this point, we have compared different ground-state *nn* relative-momentum distributions. In the next section, we

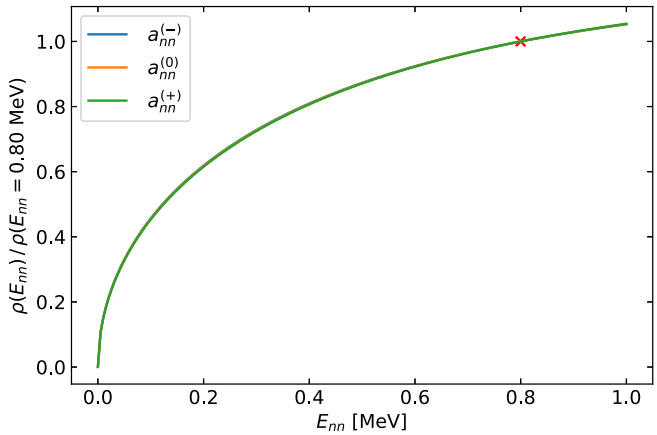

FIG. 4. Ground-state *nn* relative-energy distributions for different *nn* scattering lengths. The definitions $a_{nn}^{(+)} = -16.7$ fm, $a_{nn}^{(0)} = -18.7$ fm, and $a_{nn}^{(-)} = -20.7$ fm hold. All results are based on $\Psi_c(p, q)$. $\Lambda = 1500$ MeV was used. Based on a comparison with a calculation with half as many mesh points and $\Lambda = 1000$ MeV the numerical uncertainty is negligible. In order to be independent of the normalization the distribution is divided by its value at a certain position, which is indicated by a red cross.

will show *nn* relative-energy distributions after taking *nn* final-state interactions into account. Before we do that, we want to show what an intermediate step of this procedure looks like.[5] We show the ground-state *nn* relative-energy distribution $\rho(E_{nn})$ with $E_{nn} = p_{nn}^2/(2\mu_{nn})$. Especially, we want to investigate the influence of a_{nn} on this distribution. The relation between the momentum and the energy distribution is

$$\rho(E_{nn}) = \sqrt{\frac{\mu_{nn}}{2E_{nn}}}\rho(\sqrt{2\mu_{nn}E_{nn}}), \tag{22}$$

where we use the common style to distinguish the different variants of the function, i.e., the different functions differ only by their arguments. The necessity of the additional factor can be seen from dimensional analysis. The factor follows from a substitution in the normalization integral of the distribution. The normalization condition reads $\int dE_{nn}\rho(E_{nn}) = 1$. We plot the distribution obtained with different *nn* scattering lengths in Fig. 4.

It can be seen that the shape of the relative-energy distribution is different from the one of the momentum distribution. Additionally, we observe that the influence of the *nn* scattering length on the ground-state distribution is negligible. In contrast, we will see that, after taking the *nn* FSI into account, the distribution is sensitive to the scattering length. Thus, ^{6}He serves in the proposed experiment as a source of low-energy neutrons. Its structure is not sensitive to a_{nn}. It is the final-state *nn* interaction that enables the measurement of the scattering length.

Quantitative information on the negligible influence of the scattering length on the ground-state distribution can be found in the Supplemental Material [33]. This plot shows the ratios of the distributions obtained with different scattering lengths. They agree to better than 1%.

IV. *nn* RELATIVE-ENERGY DISTRIBUTION AFTER KNOCKOUT

The next step is to calculate the *nn* relative-energy distribution after the knockout reaction, in which the α core of ^{6}He is removed via a collision with a proton. In the experiment under discussion in this paper the knockout takes place in inverse kinematics, with a beam of ^{6}He nuclei impinging on a hydrogen target [22]. We employ the sudden approximation, i.e., we assume that the reaction mechanism is rapid and quasifree knockout of the α. Subsequent interactions between neutrons and the α or the proton that struck the α can be neglected. Therefore, in our analysis it is sufficient to treat the potential causing the knockout as an external potential. The Hilbert space for our problem is then a three-body αnn Hilbert space. Note that as an alternative to this effective three-body treatment a four-body description of this reaction is possible. The proton, which causes the knockout, would then be explicitly included in the Hilbert space. But, in our three-body treatment, that proton merely generates a potential that enables the production of the final state. We therefore refer to this as the production potential V. The quantitative properties of the final state are influenced by the *nn* potential, so that we face a two-potential scattering problem. A comprehensive discussion of such problems can be found in Refs. [31,53].

Before going into the details of that two-potential formalism and its application to α-particle knockout in ^{6}He, we want to discuss some fundamental aspects of the ^{6}He$(p, p\alpha)$ reaction. The initial state is the ground state of ^{6}He denoted by $|\Psi\rangle$. It fulfills the Schrödinger equation

$$(K_{nn} + K_{(nn)c} + V_{nn} + V_{nc} + V_{3\mathrm{B}})|\Psi\rangle = -B_3^{(0)}|\Psi\rangle, \tag{23}$$

where the kinetic energy operators are denoted by K and V_{nc} represents the interaction of the core with each of the two neutrons. In this experiment the final state is measured by a setup which detects a free *nn* state with definite relative momentum. Meanwhile, the α particle is detected at a very different angle where it is not interacting with the *nn* pair. Because of the high initial velocity of ^{6}He the neutrons will leave the α particle and proton after their interaction quickly behind, as in the laboratory frame the *nn* pair travels at almost the initial velocity of the ^{6}He beam.

Accordingly, we consider final states parametrized by the momenta p and q, that fulfill the free Schrödinger equation

$$(K_{nn} + K_{(nn)c})|p, q\rangle_c = \left(-B_3^{(0)} + E_{\mathrm{KO}}\right)|p, q\rangle_c, \tag{24}$$

[5]Note that strictly speaking the ground-state relative momentum or energy distribution is only an intermediate step in an enhancement factor based FSI approach. If the t-matrix itself is used, it has to be applied at the wave-function level. Before and after its usage the respective distributions can be calculated, but in this approach one cannot get directly from the ground-state momentum or energy distribution to the one after *nn* FSI. The details can be found in the next section.

where the energy transfer from the knockout E_{KO}, which is delivered by the proton, obeys

$$-B_3^{(0)} + E_{\mathrm{KO}} = \frac{p^2}{2\mu_{nn}} + \frac{q^2}{2\mu_{(nn)c}}. \tag{25}$$

In order for the final state to be a scattering state, the condition $E_{\mathrm{KO}} > B_3^{(0)}$ must be fulfilled. Note that energy is still conserved in the four-body ($p\alpha nn$) system. But the energy E_{KO} describes a transfer of energy into the internal (not center-of-mass) energy of the three-body system. $E_{\mathrm{KO}} < E_{\mathrm{lab},\,^6\mathrm{He}}$ then holds, where $E_{\mathrm{lab},\,^6\mathrm{He}}$ is the initial kinetic energy of the ^{6}He projectile in the laboratory frame.

Since we assume the proton interacts only with the α particle we adopt a production potential V that does not change the relative momentum of the nn pair:

$$\begin{aligned} {}_c\langle p, q|V|\Psi\rangle &= \int dp' p'^2 \int dq' q'^2 \langle p|p'\rangle \langle q|\tilde{V}|q'\rangle {}_c\langle p', q'|\Psi\rangle \\ &= \int dq' q'^2 \langle q|\tilde{V}|q'\rangle {}_c\langle p, q'|\Psi\rangle. \end{aligned} \tag{26}$$

In other words, we assume a factorization of the production potential into a nn part and a $(nn)c$ part with the nn part being an identity operator: $V = \mathbb{1} \otimes \tilde{V}$.

We now make use of the formalism of Ref. [31] for scattering from two potentials. A more detailed summary of this formalism can be found in the Supplemental Material [33]. The two potentials are taken to be the production potential V and the potential U causing the final-state interactions. We make use of a helpful identity of two-potential scattering theory for calculating the probability amplitude of the transition from a state $|\alpha\rangle$ to a state $|\beta\rangle$:

$$T_{\beta\alpha} = \langle\beta|T^{(+)}_{U+V}|\alpha\rangle. \tag{27}$$

These states satisfy the equations $H_0|\alpha\rangle = E_\alpha|\alpha\rangle$ and $H_0|\beta\rangle = E_\beta|\beta\rangle$ with $E_\alpha = E_\beta = E$. H_0 should be thought of as the part of the Hamiltonian that does not include the interactions U and V. The operator $T^{(+)}_{U+V}$ is then the t-matrix for scattering involving U and V. It satisfies the standard Lippmann-Schwinger equation, where the potential is given by $U + V$. It is possible to dissect this transition amplitude (as well as this overall t-matrix itself) into two terms by using Møller operators [31]. One of the two terms contributes for elastic scattering reactions because V, which causes the production of the final state, is missing there. We are not interested in elastic scattering here and so focus on the other term. We consider the situation in which the production potential produces a transition from a bound state to a scattering state in a subsystem. In this case V induces a transition to an eigenstate of H_0 that is orthogonal to the initial eigenstate $|\alpha\rangle$. While this discussed relation is generally a suitable starting point for the calculations, for our application we have to modify it to accommodate the case that the final-state interaction U is part of the Hamiltonian that describes the initial state. In such a case the stationary Schrödinger equation for the initial state becomes $(H_0 + U)|\alpha\rangle = E_\alpha|\alpha\rangle$. We continue to assume a free final state, so $H_0|\beta\rangle = E_\beta|\beta\rangle$ stays unchanged. Goldberger and Watson show in Ref. [31] that under these assumptions we have

$$T_{\beta\alpha} = \langle\beta|(\Omega_U^{(-)})^\dagger V(\mathbb{1} + (E - K - U - V + i\epsilon)^{-1}V)|\alpha\rangle, \tag{28}$$

where the Møller operator corresponding to the potential U is denoted by $\Omega_U^{(-)}$.

Now we have to evaluate Eq. (28). While we can (and will) evaluate it directly using the already mentioned assumption about V, this expression has also often been evaluated via FSI enhancement factors. In the next subsection we give a brief overview of this approach.

A. FSI enhancement factors

The FSI enhancement factors are a technique for approximately calculating the effect of the final-state interaction on the transition probability. The production potential is not explicitly taken into account. These enhancement factors as a generic tool were introduced by Watson [28] as well as by Migdal [29]. Watson used the approach of two-potential scattering theory to derive a relation similar to Eq. (28) and from it the enhancement factor. A detailed explanation of this way of establishing enhancement factors can be found in Ref. [31].

In this context, it is important to note that enhancement factors were introduced for describing reactions such as $\pi^- + d \to n + n + \gamma$ [54]. Here the nn enhancement factor enters in a fundamentally different way than it does in ^{6}He. In the radiative pion capture reaction the production potential and the final-state interaction both affect the same subsystem, i.e., the nn system in this case. In contrast when a high-momentum ^{6}He impinges on a proton target the production potential acts in a different subsystem than does the final-state interaction. Here we first discuss the original use case, where both V and U act on the same subsystem. We then discuss the implications for how these factors should be computed in the case of the reaction we are interested in.

The enhancement factors can be derived from Eq. (28) by using a state of definite momentum as the final state and the bound state as the initial state: $|\beta\rangle = |\boldsymbol{p}\rangle$ and $|\alpha\rangle = |\Psi\rangle$. During this derivation it is assumed that the production potential is weak and so the operator given by the expression in the brackets to the right of the first V in Eq. (28) can be approximated by $\mathbb{1}$. Additionally, it is assumed that production potential is local and only s-wave interactions are taken into account. Furthermore, it is required that the initial-state wave function and/or the production potential peak at short distances. If these conditions are satisfied one arrives at the following expression for the final momentum distribution:

$$\rho^{(G_i)}(p) \propto G_i(p)\rho(p), \tag{29}$$

where $G_i(p)$ is the enhancement factor and $\rho(p)$ is the momentum-space probability distribution from the initial (bound) state. Note that to obtain this expression we assumed that the production potential does not alter the momentum p. For the application we have in mind here this assumption holds, because the production potential and FSI potential act in different subsystems.

Different enhancement factors can be derived depending on the particular assumptions made, especially in regard to the short-distance behavior of the production potential and/or initial-state wave function. This is why we added the index i to the enhancement factor $G_i(p)$. A common variant of this enhancement factor, derived in Ref. [31], is[6]

$$G_1(p) = \frac{((p^2+\alpha^2)r_{nn}/2)^2}{\left(-\frac{1}{a_{nn}}+\frac{r_{nn}}{2}p^2\right)^2+p^2}, \tag{30}$$

where $\alpha = 1/r_{nn}(1+\sqrt{1-2r_{nn}/a_{nn}})$. This enhancement factor is based on the assumption that $V|\Psi\rangle$ peaks at $r=0$. It is also possible to derive enhancement factors for the case that $V|\Psi\rangle$ peaks at some other radius $\tilde{r}$. Further discussion regarding the derivation of the enhancement factor and how to obtain it for a general $\tilde{r}$ can be found in the Supplemental Material [33]. It contains also a discussion of the factor from Ref. [55].

So far this discussion of enhancement factors focused on two-body systems. To close this section we point out that this formalism can also be used in n-body systems. That extension assumes that the FSI is a two-body interaction within one specific particle pair; the requirement regarding the short-distance behavior then applies to the corresponding two-body subsystem of the n-body state. For a system with $n>2$ the $\rho(p)$ in Eq. (29) is the momentum-space probability distribution of the bound state after all other momenta are integrated out. Furthermore, since the FSI enhancement factor factorizes the FSI from the action of the production potential, it can be used not only in the case where the production potential acts in the same subsystem as the FSI potential, but also in cases where the two act on different subsystems of the overall n-body system.

B. Explicit calculation of rescattering

Having discussed the FSI enhancement factors in the previous subsection, we now turn our attention to the direct calculation of the wave function after FSI. Our starting point is again Eq. (28) except that now we consider it in the context of the breakup of a three-particle state into an nn pair and a residual cluster, like an α particle. For concreteness we consider the final state $\langle\beta|$ to be the free state of the nn pair and the α particle and specify that state via the relative momentum within the nn pair, p, and the momentum of the α particle relative to the nn pair, q, as well as the partial-wave quantum numbers Ω. The state is ${}_c\langle p,q;\Omega|$. The initial state $|\alpha\rangle$ is given by the ^{6}He bound state $|\Psi\rangle$. Using the notation of Eq. (23), this implies that the final state is an eigenstate of $H_0 = K_{nn}+K_{(nn)c}$, while the initial state is an eigenstate of $H_0+V_{nn}+V_{nc}+V_{3B}$. That implies that the FSI potential U is given by $V_{nn}+V_{nc}+V_{3B}$. This reflects the fact that in addition to nn interactions also nc interactions as well as three-body interactions are possible final-state interactions happening after the knockout. However, due to the kinematics of the reaction and the halo structure of ^{6}He, final-state nc or three-body interactions should be strongly suppressed. Accordingly, in the context of this calculation we approximate $\Omega_U^{(-)}$ by $\Omega_{V_{nn}}^{(-)}$. We obtain

$$\begin{aligned}\mathcal{T}_\Omega(p,q) = {}&{}_c\langle p,q;\Omega|(\Omega_U^{(-)})^\dagger V \\ &\times(\mathbb{1}+(E-K-U-V+i\epsilon)^{-1}V)|\Psi\rangle,\end{aligned} \tag{31}$$

where U is to be approximated by the nn potential. For the energy E of the Møller operator we have to insert the energy of the final state $p^2/(2\mu_{nn})+q^2/(2\mu_{(nn)c})$. Since the FSI potential U is approximated by V_{nn} and thereby acts only in the nn subsystem, we can make use of the identity

$$\begin{aligned}&\Omega_U^{(\pm)}|p,q;\Omega\rangle_c \\ &\quad= [\mathbb{1}+(p^2/(2\mu_{nn})+q^2/(2\mu_{(nn)c}) \\ &\qquad- K_{nn}-K_{(nn)c}-U\pm i\epsilon)^{-1}U]|p,q;\Omega\rangle_c \\ &\quad= [\mathbb{1}+(p^2/(2\mu_{nn})-K_{nn}-U\pm i\epsilon)^{-1}U]|p,q;\Omega\rangle_c,\end{aligned} \tag{32}$$

i.e., we use the fact that V_{nn} commutes with $K_{(nn)c}$, and so $K_{(nn)c}$ can be replaced by its eigenvalue for the state $|p,q;\Omega\rangle_c$. Next, since the production potential is assumed to be weak, in Eq. (31) we use only the lowest order of the operators next to $(\Omega_U^{(-)})^\dagger$, i.e., retain only the identity operator in the round brackets to the right of V in Eq. (31). Furthermore, we assume that V decouples as formulated in Eq. (26). It is then useful to express the Møller operator in terms of the t-matrix according to[7]

$$(\Omega_U^{(-)})^\dagger = \mathbb{1}+(G_0^{(-)}t_U^{(-)})^\dagger. \tag{33}$$

We set $\tilde{V}$ to $\mathbb{1}$, which implies that the momentum q in $\mathcal{T}_\Omega(p,q)$ is the $\alpha(nn)$ relative momentum before the reaction. We therefore calculate the probability amplitude as a function of the nn relative momentum after the reaction and the $\alpha(nn)$ relative momentum before the reaction. Another implication of not using an explicit expression for $\tilde{V}$ is that we do not take into account that the overall probability of the knockout is smaller than 1. The implications of this on the analysis are discussed in Sec. IV C, and will be accounted for by not trying to compute the absolute number of nn pairs produced, but only the shape of the distribution.

Under these assumptions the probability amplitude $\mathcal{T}_\Omega(p,q)$, which can also be seen as a final-state wave function in an arbitrary partial wave Ω after knockout and FSI, is given by

$$\begin{aligned}&\Psi_c^{(\mathrm{wFSI};\Omega)}(p,q) \\ &\quad= {}_c\langle p,q;\Omega|(\mathbb{1}+t_{nn,(\Omega)_{nn}}(E_p)G_0^{(nn)}(E_p))|\Psi\rangle \\ &\quad= \int dp' p'^2 {}_c\langle p,q;\Omega|\left(\mathbb{1}+t_{nn,(\Omega)_{nn}}(E_p)G_0^{(nn)}(E_p)\right) \\ &\qquad\times|p',q;\Omega\rangle_c\langle p',q;\Omega|\Psi\rangle,\end{aligned} \tag{34}$$

[6]Note that in Ref. [31] the enhancement factor has $1/a_{nn}$ instead of $-1/a_{nn}$ in the denominator. This is rooted in a different sign convention for the scattering length. We define $k\cot(\delta_0(k)) = -1/a_0 + r_0k^2/2+\mathcal{O}(k^4)$.

[7]We use here that $\Omega_U^{(-)}$ acts on an eigenstate of H_0. For the general form of the Møller operator see Refs. [33,56].

where the multi-index $(\Omega)_{nn}$ is the *nn* part of the multi-index Ω.

The *nn* FSI is only significant in the $^1S_0$ partial wave, so we use only the wave-function component $\Psi_c(p,q) \coloneqq {}_c\langle p,q;\Omega_c|\Psi\rangle$ for calculating the wave function after FSI. The *nn* part of this wave function's multi-index is $l=0$, $s=0$ corresponding to the $^1S_0$ channel. Accordingly, to obtain results for $\Psi_c^{(\mathrm{wFSI})}(p,q)$ a version of Eq. (34) specific to FSI in this *nn* partial wave is used:

$$\Psi_c^{(\mathrm{wFSI})}(p,q) = \Psi_c(p,q) + \frac{2}{\pi} g_0(p) \frac{1}{a_{nn}^{-1} - \frac{r_{nn}}{2}p^2 + ip} \int dp' p'^2 g_0(p') (p^2 - p'^2 + i\epsilon)^{-1} \Psi_c(p',q) \tag{35}$$

$$= \Psi_c(p,q) + \frac{2}{\pi} g_0(p) \frac{1}{a_{nn}^{-1} - \frac{r_{nn}}{2}p^2 + ip} \left[\int_0^\Lambda dp' \frac{p'^2 \Psi_c(p',q) - p^2 \Psi_c(p,q)}{p^2 - p'^2} - \left(\frac{i\pi}{2} - \frac{1}{2} \ln\left(\frac{\Lambda + p}{\Lambda - p} \right) \right) g_0(p) p \Psi_c(p,q) \right]. \tag{36}$$

Note that $\Psi_c(p,q)$ is the wave function corresponding to the momentum distribution computed in the previous section. The last equality holds in the case of Heaviside functions as regulators using the cutoff Λ: $g_l(p) = p^l \Theta(\Lambda - p)$. An auxiliary calculation can be found in the Supplemental Material [33]. Note that in the calculation leading to Eq. (36) we included the effective-range term in the *nn* t-matrix in order to check its influence. The *nn* relative-energy distribution below $E_{nn} = 1.0$ MeV that is obtained with the choice $r_{nn} = 0$ in the FSI *nn* t-matrix differs only slightly from the distribution obtained when the nominal effective range of $r_{nn} = 2.73$fm is used there. (See Fig. 7 in Appendix B.)

This procedure for calculating the FSI is common and *inter alia* used for pion capture reactions with deuterium; see, e.g., Ref. [57]. It is also similar to the coherent FSI three-body model for the sudden breakup of two-neutron halos in collisions with heavy targets developed in Ref. [58]. This model was compared to experimental data on the *nn* correlation in the breakup of ^{11}Li [59,60], ^{14}Be [59,61], and ^{6}He [59]. Within our discussion we were able to show the close connection of this method to two-potential scattering theory. Additionally, we reviewed the specific approximations which were made.

It is interesting to note that certain FSI enhancement factors can be derived from Eq. (35) by approximating the integral that appears there. This is not really surprising, since enhancement factors and this more exact calculation are both based on the findings of two-potential scattering theory. Nevertheless, the derivation elucidates the relationship of the enhancement-factor and explicit-calculation approaches to *nn* FSI and provides a different perspective on the enhancement factors. It is discussed in the Supplemental Material [33].

After applying the FSI, the absolute value of the wave function can be calculated, the integral measure can be applied, and the q momentum can be integrated out in order to obtain the probability density distribution as a function of the *nn* relative momentum, p. Note that taking $\tilde{V}$ into account in Eq. (26) could distort the probability distribution in p, even though $\tilde{V}$ acts only in the q subspace of the Hilbert space. However, such effects are expected to be small, due to the kinematics of the proposed knockout reaction. The formula for the probability density $\rho^{(t)}(p)$ in this approach (where the superscript denotes that the FSI is computed via the t-matrix) reads

$$\rho^{(t)}(p) = \int dq p^2 q^2 \left| \Psi_c^{(\mathrm{wFSI})}(p,q) \right|^2. \tag{37}$$

The relative-energy distribution can then be calculated from the momentum distribution by using Eq. (22).

The density $\rho^{(t)}(p)$ obeys the normalization condition $\int dp \rho^{(t)}(p) = 1$. However, we remind the reader that the existence of other channels than this one is not taken into account in our calculation. Thus, this normalization condition does not represent the actual probability of knockout, which in reality will be <1. Additionally, this normalization condition requires that the wave-function component in use, i.e., $\Psi_c(p,q) \coloneqq {}_c\langle p,q;\Omega_c|\Psi\rangle$, be normalized to 1, which is another approximation.

C. Comparison of results

In Fig. 5 we compare results for the *nn* relative-energy distribution obtained with the enhancement factor G_1 and with the t-matrix treatment of FSI. We do this for three different *nn* scattering lengths, for which we use the following shorthand notation:

$$a_{nn}^{(+)} = -16.7 \text{ fm}, \quad a_{nn}^{(0)} = -18.7 \text{ fm}, \quad a_{nn}^{(-)} = -20.7 \text{ fm}. \tag{38}$$

As mentioned before, we do not calculate the absolute value of the distribution, but its shape. Therefore we normalize the distribution to a certain value at a certain position. Here we normalized to 1 at $E_{nn} \approx 0.8$ MeV. Not knowing the absolute value is no problem for determining the scattering length; the distribution will be fitted to the experimental data on the spectrum and the scattering length extracted from the shape.

It can be seen that the scattering length has a significant influence on that shape. When using distributions normalized to an arbitrary value at $E_{nn} \approx 0.8$ MeV, the main effect of the scattering length is to change the height of the peak located at relative energies of roughly 100 keV. Additionally, one can see that the two different procedures to include FSI yield curves of similar shape, but they are not quantitatively

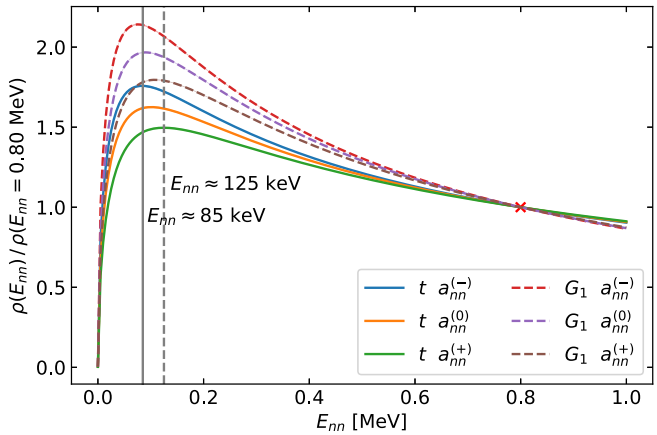

FIG. 5. Comparison of *nn* relative-energy distributions for different *nn* scattering lengths obtained with different FSI schemes. The calculation using the *nn* t-matrix is labeled as "t." $r_{nn} = 2.73$ fm is used. All results are computed using the projection $\Psi_c(p, q)$ and $\Lambda = 1500$ MeV. Uncertainty bands based on comparison with calculation with half as many mesh points and $\Lambda = 1000$ MeV are negligible. In order to be independent of the normalization the distribution is divided by its value at the energy indicated by the red cross. The solid and dashed vertical lines indicate the approximate positions of the maxima in the t-matrix based FSI scheme for $a_{nn}^{(-)}$ and $a_{nn}^{(+)}$, respectively.

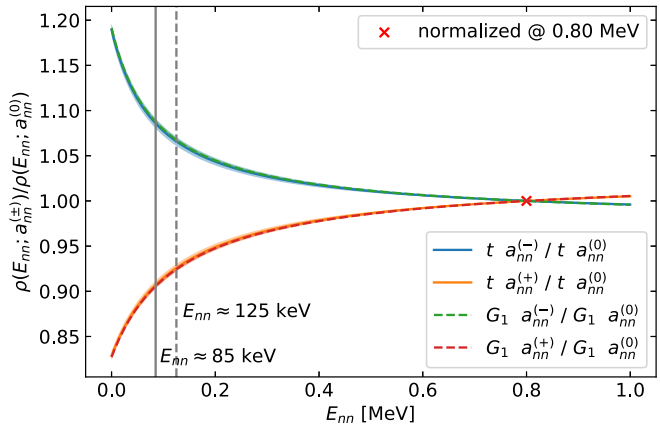

FIG. 6. Ratios of *nn* relative-energy distributions obtained with different scattering lengths for different FSI schemes in comparison. The calculation using the *nn* t-matrix is labeled as "t," and $r_{nn} = 2.73$ fm is used. All results are based on $\Psi_c(p, q)$. $\Lambda = 1500$ MeV was used. Uncertainty bands based on comparisons with calculation with half as many mesh points and $\Lambda = 1000$ MeV are shown. Due to a normalization of the distributions to a value of 1 at $E_{nn} \approx 0.8$ MeV, the quotients are at this point 1. The vertical lines indicate the approximate positions of the maxima in the t-matrix based FSI scheme for the lower and upper value of the scattering length.

in agreement. At a given a_{nn} the different FSI treatments produce different peak heights in the *nn* distribution. The enhancement-factor approach makes additional approximations beyond those involved when the *nn* FSI is fully calculated from the *nn* t-matrix. Therefore we trust the latter approach—with its full inclusion of the *nn* FSI—more.

We also calculated the distribution with the *nn* subsystem in the $^3P_1$ partial wave by applying Eq. (34) to the $\Omega_c^{(1,1,1)}$ ground-state wave-function component obtained with FaCE in setting LGM1. We found that this distribution is suppressed by a factor of at least 30 compared to the $^1S_0$ distribution (in the $E_{nn} < 1$ MeV region). We compared the ground-state distributions as well and found that FSI increased the suppression as anticipated at the beginning of Sec. III.

V. FROM THE *nn* RELATIVE-ENERGY DISTRIBUTION TO THE *nn* SCATTERING LENGTH

After showing results for the *nn* relative-energy distribution, we want to discuss in more detail how the scattering length can be extracted. Also, we want to discuss the role of the *nn* effective range. First, we quantify the influence of changing the scattering length by 2 fm. Figure 6 shows quotients of the relative-energy distributions obtained with different scattering lengths.

It can be seen that, if our normalization scheme is used, a change of the scattering length by 2 fm changes the peak height by approximately 10%. This change is almost completely independent of the method used to calculate the FSI. Additional calculations show that a change in the scattering length of 0.2 fm changes the peak height by about 1%.

In order to determine the scattering length at high precision it is necessary to know the influence of the *nn* effective range on the distribution. As with the scattering length, the effective range can enter the calculation at two stages. The first is the calculation of the ground-state wave function of ^{6}He. At this level, the influence of the scattering length is low. As the scattering length is a leading-order parameter and the effective range is a next-to-leading-order parameter, we expect its influence on the ^{6}He wave function to be very small. The second stage is taking the FSI into account. In this step, the scattering length plays a significant role. Therefore, we cannot exclude a non-negligible influence of the range in this step. We investigate the influence of the effective range in the t-matrix based FSI approach and in the approach employing the enhancement factor G_1 by using the following values:

$$r_{nn}^{(+)} = 3.0 \text{ fm}, \quad r_{nn}^{(0)} = 2.73 \text{ fm}, \quad r_{nn}^{(-)} = 2.0 \text{ fm}, \tag{39}$$

which is a rather large variation around the common literature value of $r_{np}(^1S_0) = 2.73(3)$ fm $\approx r_{\text{nn}}$ [62]. Note that we included r_{nn} only in the calculation of the FSI but not in the calculation of the ground-state wave function, as its influence there should be negligible. While the effective range is varied from $r_{nn}^{(-)}$ to $r_{nn}^{(+)}$ the change in the distribution is small: less than 1% at peak position. Details can be seen from Fig. 7 in Appendix B.

As a conclusion, these results show that the scattering length has a significant influence on the *nn* relative-energy distribution and that the effective range does not. Thus, the distribution is suitable for extracting the scattering length.

VI. OUTLOOK

Already at its present accuracy our calculation will be able to provide a precise determination of the *nn* scattering length using data from the measurement of the ^{6}He$(p, p\alpha)nn$ reaction that has been approved at RIKEN [22]. We also plan to increase the accuracy of the EFT calculation, i.e., make the uncertainty band narrower. First, we will move to NLO Halo EFT calculations of the ground-state wave function. While at $E_{nn} = 1$ MeV the LO uncertainty is approximately 20%, the NLO uncertainty at this position will be around 5%. Second, we also want to improve the treatment of the final-state interaction in EFT. For this purpose we will develop an EFT framework for knockout reactions like the one considered here. This will enable the inclusion of both the $n\alpha$ interaction after knockout and corrections to the assumption that the α particle removal does not affect the *nn* relative-energy distribution—or at least it will allow us to constrain such effects as occurring at a high order in a small expansion parameter. The resulting EFT approach to the entire ^{6}He$(p, p\alpha)nn$ reaction will allow us to rigorously assess the full uncertainty of the two-step calculation we have carried out here.

The reaction $t(p, 2p)2n$ would also facilitate a measurement of the *nn* scattering length along the same lines as those discussed in this paper. This would be a valuable reaction to examine: using two different nuclei as neutron sources checks the reliability of the result for the scattering length. As in the case of ^{6}He the ground-state wave function of the triton can be calculated in an EFT. In the case of the triton it is the well-established pionless EFT, in which the neutron and proton are the low-energy degrees of freedom [63]. This EFT has the advantage that there is no relevant *p*-wave interaction, but the triton has a two-neutron separation energy of 8.48 MeV and so is more strongly bound than ^{6}He. The treatment of its proton-induced breakup would thus involve a bigger expansion parameter and larger uncertainties at the same order as in the case of the EFT for ^{6}He. This, though, is compensated by the fact that the pionless EFT for the triton is established up to N^{2}LO [64].

ACKNOWLEDGMENTS

T.A., H.-W.H., and M.G. acknowledge support by Deutsche Forschungsgemeinschaft (DFG, German Research Foundation) - Project-ID 279384907 - SFB 1245. T.F. was a Fulbright Scholar visiting the University of Iowa at Ames when this work started and acknowledges the hospitality received, and also Conselho Nacional de Desenvolvimento Científico e Tecnológico (CNPq) Grant No. 308486/2015-3, Fundação de Amparo à Pesquisa do Estado de São Paulo (FAPESP) Project No. 2017/05660-0, INCT-FNA Project No. 464898/2014-5, and Coordenação de Aperfeiçoamento de Pessoal de Nível Superior-Brazil (CAPES-Finance Code 001). C.A.B. is partially supported by the U.S. Department of Energy Grant No. DE-FG02-08ER41533 and funding contributed by the LANL Collaborative Research Program by the Texas A&M System National Laboratory Office and Los Alamos National Laboratory. D.R.P. acknowledges support from the U.S. Department of Energy (Contract No. DE-FG02-93ER40756) and the ExtreMe Matter Institute.

APPENDIX A: CALCULATION OF WAVE FUNCTIONS IN HALO EFT

Here we describe, how wave functions of the type

$$\Psi_i(p, q) \coloneqq {}_i\langle p, q; \Omega_i|\Psi\rangle \tag{A1}$$

can be calculated starting from the $F_i(q)$ that are the solutions of the integral equations obtained using the Faddeev formalism in our Halo EFT approach. The procedure is not specific to Halo EFT; it is a general procedure for Faddeev equations in momentum space. However, in the course of this description we use identities specific to ^{6}He, mainly affecting the partial-wave states. In this context, Ω_i is the multi-index specifying the quantum numbers of the three-body system with particle i as a spectator under the condition that the total quantum numbers are the ones of the ^{6}He ground state and the numbers for the jk subsystem characterize the interaction channel. The basics of the Faddeev equations are described, e.g., in Ref. [46]. Additionally, we use results and notation of Ref. [24].

Making use of the decomposition of the total state $|\Psi\rangle$ described in Eq. (13), we can write

$$\Psi_i(p, q) \coloneqq {}_i\langle p, q; \Omega_i|\Psi\rangle = \sum_j {}_i\langle p, q; \Omega_i|\psi_j\rangle, \tag{A2}$$

whereby $|\psi_i\rangle \coloneqq G_0 t_i|F_i\rangle$ holds. In an intermediate step, we calculate

$$\begin{aligned}\psi_i(p, q) \coloneqq {}_i\langle p, q; \Omega_i|\psi_i\rangle &= 4\pi G_0^{(i)}\big(p, q; -B_3^{(0)}\big) \\ &\times g_{l_i}(p)\tau_i\big(q; -B_3^{(0)}\big)F_i(q),\end{aligned} \tag{A3}$$

where Eqs. (14)–(16) as well as the definition $\tau_i(q; E_3) \coloneqq \tau_{jk}(E_3 - \frac{q^2}{2\mu_{i(jk)}})$ were used. Additionally, $G_0^{(i)}(p, q; E_3) \coloneqq (E_3 - p^2/(2\mu_{jk}) - q^2/(2\mu_{i(jk)}))^{-1}$ holds. Consequently we have a relation between $\psi_i(p, q)$ and the numerically determined $F_i(q)$. We use this result to continue the calculation of the wave function of the total state:[8]

[8]Note that there might be additional nonvanishing wave functions $\Psi_i^{(\Omega)}(p, q) \coloneqq {}_i\langle p, q; \Omega|\Psi\rangle$ where Ω is a fixed multi-index not contained in the set of Ω_i, which are the quantum numbers of the interaction channels. These $\Psi_i^{(\Omega)}(p, q)$ are calculated as described in Eq. (A4) with the modification that the Ω_i (not the Ω_j) has to be replaced by the Ω of interest. Since this multi-index Ω has no index naming it, we would call f_{ij} now $f_{\Omega ij}$. (The κ functions are independent of Ω.) We calculated such wave functions, e.g., a $\Psi_c^{(\Omega)}(p, q)$ for $\Omega = \Omega_c^{(0,2,2)}$ and one for $\Omega = \Omega_c^{(1,1,1)}$ (notation from Sec. II).

$$\Psi_i(p,q) = \sum_j {}_i\langle p,q;\Omega_i|\psi_j\rangle = \sum_j \int dp' p'^2 \int dq' q'^2 \underbrace{{}_i\langle p,q;\Omega_i|p',q';\Omega_j\rangle_j}_{=\int dx f_{ij}(p,q,x)\delta(p'-\kappa_{ijp}(p,q,x))\delta(q'-\kappa_{ijq}(p,q,x))/(p'^2q'^2)} \psi_j(p',q')$$

$$= \sum_j \int dx f_{ij}(p,q,x)\psi_j(\kappa_{ijp}(p,q,x),\kappa_{ijq}(p,q,x)), \tag{A4}$$

where we used ${}_j\langle p,q;\Omega|\psi_j\rangle = \delta_{\Omega,\Omega_j}\psi_j(p,q)$, which follows from the properties of the used t-matrices and denoted $\cos\theta_{\boldsymbol{p},\boldsymbol{q}}$ as x. For the momenta κ_{ijk} ($k \in \{p,q\}$) we use the notation of Appendix B.1 from Ref. [24]. Formulas for the overlaps and therefore implicitly also for the $f_{ij}(p,q,x)$ are given in Appendix B.4 of that reference. We evaluate the angular integral numerically; the formula is based on simplifications described in Appendix B.2 of Ref. [24]. Note that the antisymmetrization under *nn* permutation causes some complications, but is just a special case of the more general structure described before.

The specific expression for $\Psi_c(p,q)$ we are using then reads

$$\Psi_c(p,q) = 2\pi \int_{-1}^{1} d\cos\theta_{\boldsymbol{p},\boldsymbol{q}} \left(a_c \frac{\sqrt{2}}{4\pi} (\hat{\boldsymbol{\kappa}}_{cnp}\cdot\hat{\boldsymbol{\kappa}}_{cnq}) + \tilde{a}_c \frac{\sqrt{2}}{4\pi} (\hat{\boldsymbol{\kappa}}'_{cnp}\cdot\hat{\boldsymbol{\kappa}}'_{cnq}) + \frac{d_c}{4\pi} \right). \tag{A5}$$

We use the following definitions:

$$a_c \coloneqq \psi_n(\kappa_{cnp},\kappa_{cnq}), \quad \tilde{a}_c \coloneqq \psi_n(\kappa'_{cnp},\kappa'_{cnq}), \quad d_c \coloneqq \psi_c(p,q). \tag{A6}$$

Note that $\hat{\boldsymbol{\kappa}}_{cnp}$, $\hat{\boldsymbol{\kappa}}_{cnq}$, $\hat{\boldsymbol{\kappa}}'_{cnp}$, $\hat{\boldsymbol{\kappa}}'_{cnq}$ and thereby also the "coefficients" a, $\tilde{a}$, and d depend on the momenta p and q and in general also on $x = \cos\theta_{\boldsymbol{p},\boldsymbol{q}}$. E.g., $a_c = \psi_n(\kappa_{cnp}(p,q,x),\kappa_{cnq}(p,q,x))$ holds.

APPENDIX B: INFLUENCE OF THE *nn* EFFECTIVE RANGE ON THE *nn* RELATIVE-ENERGY DISTRIBUTION

For the planned experiment, also the dependency of the *nn* relative-energy distribution on the *nn* effective range is relevant. Ideally, this dependency would be small in order not to complicate extraction of the scattering length from the measured spectrum. Figure 7 shows ratios of final-state *nn* relative-energy distributions obtained with different values for the *nn* effective range. The influence of the effective range variations at the level of the ground state was neglected in these calculations; up to this point only $r_{nn} = 2.73$ fm was used there. What is shown is therefore the effect on the FSI when r_{nn} is varied by 1 fm.

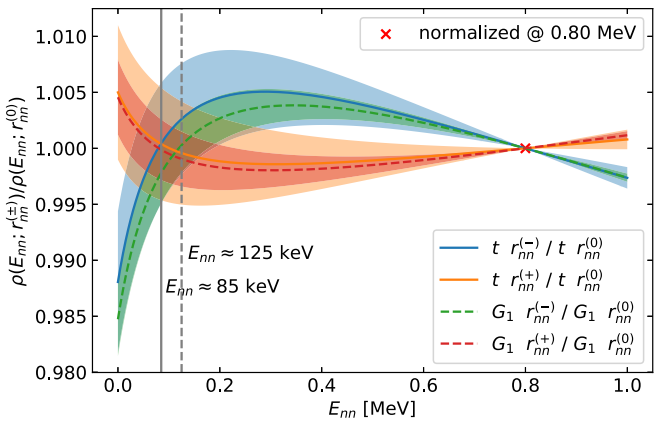

FIG. 7. Ratios of *nn* relative-energy distributions obtained with different effective ranges for different FSI schemes in comparison. The definitions $r_{nn}^{(+)} = 3.0$ fm, $r_{nn}^{(0)} = 2.73$ fm, and $r_{nn}^{(-)} = 2.0$ fm hold. All results are based on $\Psi_c(p,q)$. $\Lambda = 1500$ MeV was used. Uncertainty bands based on comparisons with calculation with half as many mesh points and $\Lambda = 1000$ MeV are shown. Due to a normalization of the distributions to a value of 1 at $E_{nn} \approx 0.8$ MeV, the quotients are at this point 1. The vertical lines indicate the approximate positions of the maxima in the t-matrix based FSI scheme for the lower and upper value of the scattering length.

The overall variation of the effective range by 1 fm has only a small influence on the distribution. The changes caused by this variation are less than 1% at the peak position. The bands showing the numerical uncertainty may appear large, but their absolute size is of the same order as in Fig. 6. However, they cover large parts of the plot because of the small influence of the effective range.

Finally, we explain how these numerical uncertainties of ratios of distributions were estimated in Figs. 6 and 7: The numerical uncertainty of the ratio r of distributions $\rho^{(1)}$ and $\rho^{(2)}$ given by

$$r(E_{nn}) \coloneqq \rho^{(1)}(E_{nn})/\rho^{(2)}(E_{nn}) \tag{B1}$$

was estimated according to

$$\Delta r(E_{nn}) = \sqrt{\left(\frac{\Delta\rho^{(1)}(E_{nn})}{\rho^{(2)}(E_{nn})}\right)^2 + \left(\frac{-\rho^{(1)}(E_{nn})}{(\rho^{(2)}(E_{nn}))^2}\Delta\rho^{(2)}(E_{nn})\right)^2} \tag{B2}$$

by using the uncertainties of the distributions denoted by $\Delta\rho^{(1)}$ and $\Delta\rho^{(2)}$. That is the standard formula for the propagation of uncertainties based on the linearization of the functions under the assumption that the two distributions are not correlated. If we would assume a correlation of 1 between the distributions (for all energies), the uncertainty bands would get much smaller. While this might be a reasonable approximation, we chose to draw more pessimistic uncertainty bands by not using it.

[1] G. A. Miller, A. K. Opper, and E. J. Stephenson, Ann. Rev. Nucl. Part. Sci. **56**, 253 (2006).
[2] A. Gårdestig, J. Phys. G **36**, 053001 (2009).
[3] R. Machleidt and I. Slaus, J. Phys. G **27**, R69 (2001).
[4] A. Gårdestig and D. R. Phillips, Phys. Rev. C **73**, 014002 (2006).
[5] V. Huhn, L. Wätzold, C. Weber, A. Siepe, W. von Witsch, H. Witała, and W. Glöckle, Phys. Rev. Lett. **85**, 1190 (2000).
[6] R. Machleidt, Phys. Rev. C **63**, 024001 (2001).
[7] W. von Witsch, X. Ruan, and H. Witała, Phys. Rev. C **74**, 014001 (2006).
[8] D. E. Gonzalez Trotter *et al.*, Phys. Rev. Lett. **83**, 3788 (1999).
[9] D. E. Gonzalez Trotter *et al.*, Phys. Rev. C **73**, 034001 (2006).
[10] B. Gabioud *et al.*, Phys. Rev. Lett. **42**, 1508 (1979).
[11] B. Gabioud *et al.*, Phys. Lett. B **103**, 9 (1981).
[12] B. Gabioud *et al.*, Nucl. Phys. A **420**, 496 (1984).
[13] O. Schori, B. Gabioud, C. Joseph, J. P. Perroud, D. Rüegger, M. T. Tran, P. Truöl, E. Winkelmann, and W. Dahme, Phys. Rev. C **35**, 2252 (1987).
[14] C. R. Howell *et al.*, Phys. Lett. B **444**, 252 (1998).
[15] V. Huhn, L. Wätzold, C. Weber, A. Siepe, W. von Witsch, H. Witała, and W. Glöckle, Phys. Rev. C **63**, 014003 (2000).
[16] Q. Chen *et al.*, Phys. Rev. C **77**, 054002 (2008).
[17] C. Bäumer *et al.*, Phys. Rev. C **71**, 044003 (2005).
[18] C. Tzara, Nucl. Phys. A **256**, 381 (1976).
[19] G. Fäldt and U. Tengblad, Phys. Scripta **34**, 742 (1986).
[20] V. Lensky, V. Baru, E. Epelbaum, C. Hanhart, J. Haidenbauer, A. E. Kudryavtsev, and U.-G. Meissner, Eur. Phys. J. A **33**, 339 (2007).
[21] S. X. Nakamura, T. Ishikawa, and T. Sato, arXiv:2003.02497.
[22] T. Aumann *et al.*, Proposal for a nuclear-physics experiment at the RI beam factory: Determination of the *nn* scattering length from a high-resolution measurement of the *nn* relative-energy spectrum produced in the ^{6}He$(p, p\alpha)^2n$, $t(p, 2p)^2n$, and $d(^7$Li, ^{7}Be$)^2n$ reactions, Proposal No. NP2012-SAMURAI55R1, 2020 (unpublished).
[23] C. Ji, C. Elster, and D. R. Phillips, Phys. Rev. C **90**, 044004 (2014).
[24] M. Göbel, H.-W. Hammer, C. Ji, and D. R. Phillips, Few Body Syst. **60**, 61 (2019).
[25] L. V. Chulkov, B. V. Danilin, A. Korsheninnikov, and M. V. Zhukov, Nucl. Phys. A **533**, 428 (1991).
[26] M. V. Zhukov, B. V. Danilin, D. V. Fedorov, J. M. Bang, I. J. Thompson, and J. S. Vaagen, Phys. Rept. **231**, 151 (1993).
[27] I. J. Thompson, F. M. Nunes, and B. V. Danilin, Comput. Phys. Commun. **161**, 87 (2004).
[28] K. M. Watson, Phys. Rev. **88**, 1163 (1952).
[29] A. B. Migdal, Zh. Eksp. Teor. Fiz. **28**, 3 (1955) [Sov. Phys. JETP. **1**, 2 (1955)].
[30] R. J. Slobodrian, Rept. Prog. Phys. **34**, 175 (1971).
[31] M. L. Goldberger and K. M. Watson, *Collision Theory* (Dover, New York, 2004).
[32] M. Brodeur *et al.*, Phys. Rev. Lett. **108**, 052504 (2012).
[33] See Supplemental Material at http://link.aps.org/supplemental/10.1103/PhysRevC.104.024001 for a detailed analysis of the differences between the model calculations and the leading-order EFT, a plot on the influence of the *nn* scattering length on the ground state, a detailed discussion of FSI enhancement factors, as well as additional information on the model calculations themselves.
[34] H.-W. Hammer, C. Ji, and D. R. Phillips, J. Phys. G **44**, 103002 (2017).
[35] See https://doi.org/10.17632/4g97cjzzyp.1.
[36] J.-M. Sparenberg and D. Baye, Phys. Rev. Lett. **79**, 3802 (1997).
[37] S. Sack, L. C. Biedenharn, and G. Breit, Phys. Rev. **93**, 321 (1954).
[38] L. V. Grigorenko, N. B. Shulgina, and M. V. Zhukov, Phys. Rev. C **102**, 014611 (2020).
[39] S. Ali, A. A. Z. Ahmad, and N. Ferdous, Rev. Mod. Phys. **57**, 923 (1985).
[40] G. E. Brown and A. D. Jackson, *The Nucleon-Nucleon Interaction* (North-Holland, Amsterdam, 1976).
[41] C. A. Bertulani, H.-W. Hammer, and U. Van Kolck, Nucl. Phys. A **712**, 37 (2002).
[42] P. F. Bedaque, H.-W. Hammer, and U. van Kolck, Phys. Lett. B **569**, 159 (2003).
[43] B. H. J. McKellar and C. M. McKay, Austral. J. Phys. **36**, 607 (1983).
[44] J. Formánek, R. J. Lombard, and J. Mareš, Czech. J. Phys. **54**, 289 (2004).
[45] I. R. Afnan and A. W. Thomas, Top. Curr. Phys. **2**, 1 (1977).
[46] W. Glöckle, *The Quantum-Mechanical Few-Body Problem* (Springer-Verlag, Berlin, 1983).
[47] E. Ryberg, C. Forssén, and L. Platter, Few Body Syst. **58**, 143 (2017).
[48] R. A. Arndt, D. D. Long, and L. D. Roper, Nucl. Phys. A **209**, 429 (1973).
[49] W. N. Polyzou and W. Glöckle, Few-Body Syst. **9**, 97 (1990).
[50] H. Hebach, P. Henneberg, and H. Kümmel, Phys. Lett. B **24**, 134 (1967).
[51] M. S. Shah and A. N. Mitra, Phys. Rev. C **1**, 35 (1970).
[52] A. Ghovanlou and D. R. Lehman, Phys. Rev. C **9**, 1730 (1974).
[53] M. Gell-Mann and M. L. Goldberger, Phys. Rev. **91**, 398 (1953).
[54] K. M. Watson and R. N. Stuart, Phys. Rev. **82**, 738 (1951).
[55] D. P. Boyd, P. F. Donovan, and J. F. Mollenauer, Phys. Rev. **188**, 1544 (1969).
[56] J. Taylor, *Scattering Theory: the Quantum Theory of Nonrelativistic Collisions* (Dover, New York, 2006).
[57] J. Golak, R. Skibiński, K. Topolnicki, H. Witała, A. Grassi, H. Kamada, A. Nogga, and L. E. Marcucci, Phys. Rev. C **98**, 054001 (2018).
[58] M. T. Yamashita, T. Frederico, and L. Tomio, Phys. Rev. C **72**, 011601(R) (2005).
[59] F. M. Marqués *et al.*, Phys. Lett. B **476**, 219 (2000).
[60] M. Petrascu *et al.*, Nucl. Phys. A **738**, 503 (2004).
[61] F. M. Marqués *et al.*, Phys. Rev. C **64**, 061301(R) (2001).
[62] M. A. Preston and R. K. Bhaduri, *Structure Of The Nucleus* (Addison-Wesley, Reading, MA, 1975).
[63] P. F. Bedaque, H.-W. Hammer, and U. van Kolck, Nucl. Phys. A **676**, 357 (2000).
[64] P. F. Bedaque, G. Rupak, H. W. Griesshammer, and H.-W. Hammer, Nucl. Phys. A **714**, 589 (2003).